Robust H_∞ Control of a Multivariable Experimental 4-Tank System

Rajanikanth Vadigepalli, Edward P. Gatzke and Francis J. Doyle III*

Department of Chemical Engineering
University of Delaware, Newark, DE 19716

Abstract

A multivariable laboratory process of four interconnected water tanks is considered for modeling and robust control. The objective of the current study is to design and implement a variety of control algorithms and present corresponding robust control analysis on a multivariable laboratory four tank process. The control methodologies considered are (i) decentralized PI control, (ii) "inner-outer" factorization based multivariable Internal Model Control, and (iii) μ-analysis based H_∞ control. The three control algorithms are comparatively analyzed using standard robustness measures for stability and peformance. The algorithms are implemented on the four tank system and the performance is compared in reference tracking and disturbance rejection cases. Using experimental data, the process dynamics and disturbance effects are modeled. Input-output controllability analysis is performed to characterize achievable performance. A lumped unstructured uncertainty description is utilized to represent the variations

*Author to whom correspondence should be addressed. Phone: (302) 831-0760. Fax: (302) 831-1048. E-mail: *fdoyle@udel.edu*.

in the system. The three controllers designed are implemented on the four tank experimental apparatus using a Bailey control system utilizing MATLAB and Freelance software interface. The controllers are shown to provide stable and acceptable performance for reference tracking and disturbance rejection experiments. The multivariable IMC and H_∞ controllers performed similarly and provided better performance than the decentralized PI control.

Keywords: robust multivariable control, decentralized PI control, Internal Model Control, H_∞ control, μ-analysis, four tank system.

1 Introduction

Typical chemical plants are tightly integrated processes which exhibit nonlinear behavior and complex dynamic properties. For decades, the chemical process industry has relied on single-loop linear controllers to regulate such systems. In many cases, the tuning of these controllers can be described as "heuristic". The performance of such a control design in an uncertain process environment is difficult to predict. Although a nonlinear process model of a system may be available, linear process models are usually developed for controller synthesis and system analysis. Using a linear model, an uncertainty characterization can be used to mathematically describe the model error and other variations in the system. Desirable performance criteria can be established as well. Optimal controllers can be designed using well-known tools such as H_∞ synthesis and μ-analysis [1, 2]. These robust controller design techniques have been demonstrated in various experimental process applications [3, 4, 5, 6, 7].

The four tank system has attracted recent attention as it exhibits characteristics of interest in both control research and education [8, 9, 10]. A similar process with three interconnected tanks has been utilized as a benchmark system for control research [7]. The four tank system exhibits elegantly complex dynamics which emerge from a simple cascade of tanks. Such dynamic characteristics include interactions and transmission zero location that are tunable in operation. With appropriate "tuning", this system exhibits non-minimum phase characteristics that arise completely from the multivariable nature of the problem. The four tank system has been used to illustrate both traditional and advanced multivariable control strategies [10, 11, 12] and has been utilized as an educational tool in teaching advanced multivariable control techniques [9]. The specific experiment presented in this study is significantly larger in scale than all the previously published versions of the system by approximately 1-2 orders of magnitude, and, consequently, introduces a number

of nonidealities including gravitational heads, piping friction losses, in addition to behaviors specific to large tanks such as vortices and splashing effects on level measurement, etc. These characteristics, combined with the complex interactive behavior, enable the four tank system to serve as a valuable educational tool as well as provide interesting challenges in the control design [10, 12].

The objective of the current study is to design and implement a variety of control algorithms and present corresponding robust control analysis on a multivariable laboratory four tank process. The control methodologies considered are (i) decentralized PI control, (ii) "inner-outer" factorization based multivariable Internal Model Control, and (iii) μ-analysis based H_∞ control. The three control algorithms are comparatively analyzed using standard robustness measures for stability and peformance. The algorithms are implemented on the four tank system and the performance is compared in reference tracking and disturbance rejection cases.

The particular design of the process considered in this paper is described in [9]. Two pumps are used to convey water from a basin into four overhead tanks. The two tanks at the upper level drain freely into the two tanks at the bottom level. The liquid levels in the bottom two tanks are measured. The piping system is such that each pump affects the liquid levels of both measured tanks. A portion of the flow from one pump is directed into one of the lower level tanks (where the level is monitored). The rest of the flow from a single pump is directed to the overhead tank that drains into the other lower level tank. By adjusting the bypass valves of the system, the amount of interaction between the inputs and the outputs can be varied. The process flowsheet is displayed in Figure 1. In the present study, additional flow disturbances are introduced into the upper level tanks. These external unmeasured disturbance flows can either drain or fill the top tanks. The process variations include uncertainties in the actuators, valve settings, and head losses in the tanks. The objective of the present study is to design a robustly performing controller that provides

stable and acceptable performance for flow disturbance rejection and setpoint tracking.

2 Modeling and Parameter Estimation

A nonlinear mathematical model for a similar four tank system is detailed in [11]. The model used in the present study includes the disturbance effect of flows in and out of the upper level tanks 3 and 4 as depicted in Figure 1. The differential equations representing the mass balances in this four tank system are:

$$\begin{aligned}
\frac{dh_1}{dt} &= -\frac{a_1}{A_1}\sqrt{2gh_1} + \frac{a_3}{A_1}\sqrt{2gh_3} + \frac{\gamma_1 k_1}{A_1}\nu_1 \\
\frac{dh_2}{dt} &= -\frac{a_2}{A_2}\sqrt{2gh_2} + \frac{a_4}{A_2}\sqrt{2gh_4} + \frac{\gamma_2 k_2}{A_2}\nu_2 \\
\frac{dh_3}{dt} &= -\frac{a_3}{A_3}\sqrt{2gh_3} + \frac{(1-\gamma_2)k_2}{A_3}\nu_2 - \frac{k_{d_1} d_1}{A_3} \\
\frac{dh_4}{dt} &= -\frac{a_4}{A_4}\sqrt{2gh_4} + \frac{(1-\gamma_1)k_1}{A_4}\nu_1 - \frac{k_{d_2} d_2}{A_4}
\end{aligned} \tag{1}$$

where h_i is the liquid level in tank i; a_i is the outlet cross sectional area of tank i; A_i is the cross sectional area of tank i; ν_j is the speed setting of pump j, with the corresponding gain k_j; γ_j is the portion of the flow into the upper tank from pump j; d_1 and d_2 are flow disturbances from tank 3 and tank 4 respectively, with corresponding gains k_{d_1} and k_{d_2}. The process manipulated inputs are ν_1 and ν_2 (speed settings to the pumps) and the measured outputs are y_1 and y_2 (voltages from level measurement devices). The measured level signals are assumed to be proportional to the true levels, *i.e.*, $y_1 = k_{m1}h_1$ and $y_2 = k_{m2}h_2$. The level sensors were calibrated so that $k_{m1} = k_{m2} = 1$.

This simple mass balance model adopts Bernoulli's law for flow out of the orifice. The tank areas A_i can be measured directly with adequate accuracy from the apparatus. Using tank drainage data, estimates of the cross sectional outlet areas a_i can also be determined.

The steady state operating conditions of $\nu_1 = 50\%$ and $\nu_2 = 50\%$ are used for subsequent modeling and controller synthesis. Johansson and Nunes (1998) have shown that the inverse response in the modeled outputs will occur when $\gamma_1 + \gamma_2 < 1$. In the present system, the valves were set such that the nominal operating point exhibits inverse response.

For the purpose of parameter estimation, dynamic data was collected from the laboratory system using input sequences as a series of steps in orthogonal directions, *i.e.*, $(1,1)$, $(1,-1)$, $(-1,1)$, and $(-1,-1)$. This is intended to sufficiently excite the multivariable process. To determine the model parameters, a nonlinear constrained optimization procedure that minimizes the scaled 2-norm of the difference between the nonlinear model and actual measurements is employed. This optimization formulation is represented as:

$$\min_{\gamma_j, k_j} \sum_{k=1}^{N} \|\boldsymbol{e}(k)\|_2^2 \qquad i = 1 \ldots 4 \text{ and } j = 1, 2 \tag{2}$$

where at every time instant $k = 1 \ldots N$ of the data record, each element of $\boldsymbol{e}(k) \in R^2$ is $e_j(k) = (h_j^{nl}(k) - h_j^{meas}(k))/h_j^{nl}(k)$, for $j = 1, 2$; the indices nl and $meas$ denote nonlinear model prediction and observed measurement, respectively. The optimal parameter values are computed utilizing the *constr* function in MATLAB. Parameter values computed from the steady state data were used to initialize the optimization algorithm for error minimization. Note that this optimization is nonlinear and is based on the noisy data and hence is not guaranteed to result in globally optimal parameter values. However, parameter constraints were imposed to restrict the optimization for γ_j to positive values less than 0.5 (as the nominal operating condition IS in the inverse response regime for both levels) and pump constants k_j to remain within $\pm 100\%$ of the measured steady-state calibrations. The initialization data was "perturbed" across multiple optimization runs so that the estimates are close to optimal. The nominal operating conditions and the estimated parameters of the nonlinear model are shown in Table 1. The estimated parameter values are found to be within the

constraints and are not on the constraint surface indicating that the estimates are close to "true" values. The model fit and validation results are shown in Figure 2. The residual error between experimental data and the nonlinear model are within $\pm 10\%$.

The linearized state space model for these operating conditions and parametric values is given as:

$$\dot{\boldsymbol{x}} = \begin{bmatrix} -\frac{1}{T_1} & 0 & \frac{A_3}{A_1 T_3} & 0 \\ 0 & -\frac{1}{T_2} & 0 & \frac{A_4}{A_2 T_4} \\ 0 & 0 & -\frac{1}{T_3} & 0 \\ 0 & 0 & 0 & -\frac{1}{T_4} \end{bmatrix} \boldsymbol{x} + \begin{bmatrix} \frac{\gamma_1 k_1}{A_1} & 0 \\ 0 & \frac{\gamma_2 k_2}{A_3} \\ 0 & \frac{(1-\gamma_2) k_2}{A_3} \\ \frac{(1-\gamma_1) k_1}{A_4} & 0 \end{bmatrix} \boldsymbol{u} + \begin{bmatrix} 0 & 0 \\ 0 & 0 \\ -\frac{k_{d_1}}{A_3} & 0 \\ 0 & -\frac{k_{d_2}}{A_4} \end{bmatrix} \boldsymbol{d}$$

$$\boldsymbol{y} = \begin{bmatrix} 1 & 0 & 0 & 0 \\ 0 & 1 & 0 & 0 \end{bmatrix} \boldsymbol{x} \tag{3}$$

where $\boldsymbol{x} = [h_1\, h_2\, h_3\, h_4]^T$, $\boldsymbol{u} = [\nu_1\, \nu_2]^T$, $\boldsymbol{d} = [d_1\, d_2]^T$, and $\boldsymbol{y} = [h_1\, h_2]^T$. For the linearized system, the time constants for the system are given as: $T_i = \frac{A_i}{a_i}\sqrt{\frac{2h_i^0}{g}}$. The corresponding linear transfer function matrix is:

$$G(s) = \begin{bmatrix} \frac{\gamma_1 c_1}{(T_1 s+1)} & \frac{(1-\gamma_2) c_2}{(T_1 s+1)(T_3 s+1)} \\ \frac{(1-\gamma_1) c_1}{(T_2 s+1)(T_4 s+1)} & \frac{\gamma_2 c_2}{(T_2 s+1)} \end{bmatrix} \tag{4}$$

where $c_j = \frac{T_j k_j}{A_j}$, $j = 1, 2$. Note that individual transfer functions in each of the input-output channels of $G(s)$ do not have zeros. The RHP zero of the system is a multivariable characteristic and imposes limitations on achievable performance as discussed in the next section.

Figure 2 also shows the residual error between nonlinear and linearized model with the estimated parameters. This error is well within $\pm 5\%$, indicating that the linearized model is probably sufficient for controller design. From Figure 3, it can be seen that both the linear

and the nonlinear models display inverse response for appropriate step change in the inputs (a positive change in one pump and a negative step change in the other pump).

For the disturbance model identification, submersible pumps were used in the overhead tanks to pump water out of the overhead tanks and into the lower basin. While activating the disturbance at known times, process data was collected. To determine the parameters for the disturbance flow rates, the process data was used in an optimization routine similar to the one used for model parameter estimation. The identification and validation results are shown in Figure 4.

Prior to the control analysis and controller synthesis, the manipulated inputs were scaled by 25%. This scaling corresponds to actual input levels in the range $25\% - 75\%$. Due to the nonlinearities introduced by the water head in the piping and limited pump capacities, the pumps cannot operate satisfactorily below 25% level. Hence, a larger input scaling factor could not be chosen even though the pumps could operate at more than 75%. The measured levels were scaled by 4 *cm* deviation corresponding to the maximum expected change in the liquid levels. The disturbance was scaled such that the maximum deviation obtained with the submersible pump corresponds to a disturbance of size 1. These scaling factors are listed in Table 1.

3 Input-Output Controllability Analysis

Controllability analysis is performed on the system to determine the limitations of feedback control. The following criteria were examined based on the controllability analysis procedure detailed in [2]:

- *Multivariable interactions*: The frequency dependent Relative Gain Array (RGA) elements for the linear system are displayed in Figure 5. At low frequency, the off-diagonal

elements of the RGA are of the order of 1, indicating that the decentralized control could be considered with pairings $[y_1, u_2]$ and $[y_2, u_1]$. The diagonal elements of the RGA matrix remains approximately 0.21 at low frequency. This indicates some level of interaction, but adequate control should be possible.

- *Nonminimum Phase (NMP) characteristics*: The diagonal elements of the RGA change sign from steady state to high frequency indicating the presence of an RHP zero in the system. Individual transfer function channels of $G(s)$ do not have RHP zeros. The multivariable RHP zero is found to be at 0.034 for the nominal operating conditions and is associated with the input direction $u_z = [-0.69; 0.73]$ and output direction $\nu_z = [-0.73; 0.69]$. This is consistent with the inverse response observed in the real system when forcing an increase in one pump speed while the other is decreased. The RHP zero imposes a upper bound constraint on the achievable bandwidth as $\omega_c \leq z/2$. The RHP zero direction indicates that the performance degradation can be shifted entirely to either one of the outputs [13]. The RHP zero arising out of multivariable nature of the system indicates that decentralized (or SISO) controllers have to be "retuned" for the multivariable system according to the inherent performance limitations due to NMP characteristics.

- *Sensitivity to uncertainty*: The singular values for the system as a function of frequency are plotted in Figure 5. The condition number, $\gamma(G)$, is of low order of magnitude, implying that the plant is not ill-conditioned. The condition number is higher at low frequency, indicating that the plant is more sensitive to unstructured uncertainty at the steady state than at higher frequencies.

- *Functional controllability*: The system is functionally controllable if $G(s)$ has full row rank. For a square MIMO system this condition is equivalent to $\det G(s) \neq 0, \forall s$, except at finite number of zeros of $G(s)$. The four tank system is functionally

controllable as this criterion is satisfied.

- *Input saturation*: Perfect control is achievable in the presence of combined reference changes without saturating the inputs (in terms of the 2-norm) if the following condition is satisfied [2]:

$$\underline{\sigma}(R^{-1}G) \geq 1 \qquad \forall \omega \leq \omega_r \tag{5}$$

where ω_r is the frequency up to which reference tracking is required. Alternatively, this is a limitation on achievable bandwidth for reference tracking. A similar condition for disturbance rejection is obtained by replacing R with G_d in Equation 5. In the current problem, the error scaling factor, $\overline{e}$, is chosen to be equal to reference scaling factor, $\overline{r}$. Therefore, the reference scaling matrix, $R = I$. Hence, the perfect control conditions for reference tracking are directly obtained from the singular values of G. The low frequency minimum singular value of the process, $\underline{\sigma}(j\omega)$, is greater than 1 (Figure 5). This indicates that adequate control should be possible; the input moves will be able to change the outputs by a sufficient amount, while maintaining the scaled inputs and outputs less than 1. The minimum singular value of the plant is greater than 1 up to a frequency of $\omega = 0.015$ *Hz*. This is an upper bound on the controller bandwidth, ω_c, due to input saturation considerations at high frequency. This value is dependent upon the scaling of inputs and outputs. For the disturbance rejection problem, one requires that $\underline{\sigma}(G_d^{-1}G) > 1, \forall \omega$. The current process satisfies this criterion (Figure 5). As a result, perfect control for disturbance rejection can be achieved with no limitation on the achievable bandwidth as set by the input saturation criterion. The RHP zero also imposes an upper bound constraint on the achievable bandwidth as $\omega_c \leq z/2 = 0.017$ *Hz*, for the present process. Based on the minimum singular value constraint and RHP zero limitation, the achievable bandwidth for reference tracking is 0.015 *Hz*. Note

that the two limitations almost overlap in the nominal case. This indicates that if larger input space were available, *i.e.*, $\overline{u} > 25\%$, the input saturation would occur at higher frequency and the RHP zero limitation ($\omega_c \leq 0.017$ *Hz*) would be "active". Uncertainty also plays a role in the "active" limitation on achievable bandwidth as the input saturation and RHP zero limitations vary with parameter changes. This aspect is discussed in the next section after the details of uncertainty characterization of the four tank system are presented.

An interesting ramification of the adjustable by-pass valves (varying γ_j) is that one can adjust the degree of interaction in the system. If one assumes that the system is perfectly symmetric (including the bypass, γ), it is easy to show that the (1,1) element of the RGA of the linearized model is given by:

$$\lambda = \frac{\gamma^2}{2\gamma - 1}$$

which indicates that all values of λ less than zero, and greater than one, are possible. Typically, controller design for multivariable system involves extensive analysis of interactions and corresponding "retuning" of the controllers for implementation. However, in this study, we present the case in which interactions are minimal, while at the same time the multivariable nature of the system imposes considerable performance limitations through a multivariable RHP zero. The nominal operating point is appropriately chosen so that the "retuning" of the controllers is not affected by the criteria based on multivariable interactions but is affected by limitations based on RHP zero location.

4 Uncertainty Characterization

In order to rigorously analyze the robustness properties of the system, the plant-model error must be quantified. Sources of uncertainty in the four tank system include: (1) unmodeled

and neglected dynamics, (2) valve position uncertainty, which affects the ratios of flows across the top and bottom tanks, (3) uncertainty in the actuators, and (4) nonlinearities in the system. A lumped unstructured input multiplicative uncertainty is considered. The corresponding family of linear systems considered is represented by:

$$G_p(\omega) = G(\omega)(I + W_I(\omega)\Delta_I) \tag{6}$$

where $G(\omega)$ is the nominal model, $G_p(\omega)$ is the "actual" process, $W_I(\omega)$ is the multiplicative frequency dependent uncertainty bound, and Δ_I is a linear time invariant operator whose frequency response is an arbitrary complex operator with $\|\Delta_I(\omega) = \|_\infty \leq 1$, $\forall\omega$. The closed-loop system with the real process G_p represented using this uncertainty structure is shown in Figure 6. The uncertainty bound $W_I(\omega)$ is chosen to satisfy the requirement that:

$$\|W_I(\omega)\|_\infty \geqslant \sup_{G_p(\omega)\in\Pi_I} \|G^{-1}(\omega)(G_p(\omega) - G(\omega))\|_\infty \qquad \forall\omega \tag{7}$$

where G_p is a perturbed plant and Π_I is the set of all perturbed plants. The parametric uncertainty can be rigorously characterized through least square statistics methods [14]. However, for this application, the perturbed plant G_p is obtained numerically by varying the parameters $\gamma_1, \gamma_2, k_1,$ and k_2 by $\pm 10\%$ of the corresponding nominal value. These variations are found to be sufficient to capture the changes in steady state operating level for a range of approximately $6\,cm$. This "covers" a broad spectrum of operating levels in the non-minimum phase regime. The experimental data and operational experience confirm this to be a reasonable level of uncertainty. A diagonal uncertainty weight, W_I, is considered assuming that both input channels have the same uncertainty characteristics. This is a reasonable assumption as the system is nearly symmetric, and is evident from the parameter estimates shown in Table 1. The multiplicative uncertainty weight is found to be $W_I = (\frac{s+0.40*0.12}{s/0.22+0.12})$

and corresponds to the set of perturbed processes shown in Figure 7. At steady state, the system exhibits approximately 40% uncertainty, while at higher frequencies the uncertainty drops to approximately 22%. This is in tune with the operational experience which indicates that the system exhibits similar dynamics while operating at different steady state levels in each of the minimum phase and nonminimum phase regimes. This higher uncertainty at steady state might impose limitation on the steady state performance of the system. An integrating action in the controller can overcome this limitation.

The achievable bandwidth for closed loop performance is limited by the input saturation and the RHP zero location. Figure 8 shows the variation of the minimum singular value of G and the RHP zero location. For the uncertainty considered here, the input saturation upperbound is in the range $0.01 - 0.025\ Hz$ while the RHP zero location varies in the range $0.023\ Hz$ to $0.047\ Hz$ with corresponding bandwidth limitation in the range $0.0115 - 0.0235\ Hz$. This overlap indicates that the input saturation and the RHP zero limitations are "active" separately on a per case basis within the domain of perturbed plants considered.

5 Controller Synthesis

The control algorithms considered in this work include (i) decentralized PI control (PI), (ii) multivariable Internal Model Control (IMC), and (iii) μ-analysis based H_∞ controller (H_∞). For each of the controller design, a stable controller is desired that achieves reasonable performance, given the process limitations. In the reference tracking problem, no disturbances were assumed to be present in the system. Additionally, no reference changes are assumed to occur for the distrubance rejection problem. A performance weight W_p of the following form is utilized [2]:

$$W_p(s) = \frac{s/M + \omega_B^*}{s + A\omega_B^*} \tag{8}$$

where ω_B^* is the desired controller bandwidth, A is the steady state offset, and M is a limit on the maximum value of the sensitivity function. For the H_∞ controller, the controller bandwidth ω_B^* and the peak sensitivity bound, M, are adjusted until the required performance criteria are satisfied.

Typical robust performance criteria involve computation of the sensitivity and complementary sensitivity functions. The sensitivity function S is the closed-loop operator from d to y or from r to e. The complementary sensitivity function T is the closed-loop operator from r to y and is related to the sensitivity function as $S+T = I$, where I is the identity operator. For the classical feedback structure shown in Figure 6, $S = (I + GK)^{-1}$. For the IMC control structure, $S = (I - GK)$. For each of the PI, IMC and H_∞ controllers, S and T are computed as a function of frequency and the nominal performance (NP: $\|W_p S\|_\infty < 1$), robust stability (RS: $\|W_I T\|_\infty < 1$), and robust performance (RP: structured singular value, $\mu < 1$) criteria are evaluated [15]. For each control algorithm, a robustly performing controller that is also nominally stable is designed.

5.1 Robust PI controller design

A decentralized PI controller as a combination of two SISO PI controllers is considered. Each PI controller is designed based on the relay tuning method [16]. The "auto tuning" method using a relay controller may be used to determine the stability limits of the system in terms of ultimate gain and ultimate period for small amplitude experiments. The period of the closed loop response is the ultimate period P_u and the ultimate proportional controller gain is given by $K_{cu} = \frac{4h}{\pi A}$, where h is the amplitude of the input to the system and A is the output amplitude. Once the stability limits K_{cu} and P_u are known, the Ziegler-Nichols

stability margin design could be used to calculate the parameters K_c and τ_I for the PI controller as $K_c = 0.45K_{cu}$ and $\tau_I = P_u/1.2$. The decentralized PI controller thus designed is typically "detuned" to account for multivariable interactions and to provide robust stability and performance. In the case of the four tank system, interactions are not as critical as the RHP zero and input saturation based performance limitations.

For the purpose of the decentralized PI controller design, the RGA matrix indicates that the pairing $y_1 - u_2$ and $y_2 - u_1$ is appropriate. Note that the plant has negative gain in the nonminimum phase setting, *i.e.*, determinant of G is negative. This indicates that no controller K with positive gain (determinant) will stabilize the system under negative feedback. The pairing $y_1 - u_2$ and $y_2 - u_1$ chosen after RGA analysis always results in a K with negative gain as long as each of the controllers have positive gain. So, the pairing is appropriate from the stability perspective.

Separate experiments were performed for each of the SISO pairings $y_1 - u_2$ and $y_2 - u_1$. In each case, the input is cycled within $\pm 10\%$ from the nominal operating point of 50%. This was done to minimize the effect of nonlinearities on the controller design. The input and output time profiles utilized in the controller design are shown in Figure 9. The resulting PI controllers are $[K_{c1} = 3.57, \tau_{I1} = 46.8]$, and $[K_{c2} = 3.78, \tau_{I2} = 49.3]$. Note that each of these loops is theoretically second-order and hence do not have theoretical stability limits. This means that the resulting PI controller is very aggressively tuned and does not provide stable nominal performance when employed on the multivariable system. This is due to violation of the bandwidth limitation imposed by the RHP zero and the input saturation criteria. The controllers need to be detuned to conform to these limitations. Also, the NP, RS and RP criteria have to be satisfied. The PI controller is detuned through an iterative *ad hoc* trial and error procedure. Figure 10 shows that the detuned decentralized PI controller satisfies the NS, RS and RP criteria for robust performance. This controller has a μ-value of 0.99 satisfying the robust performance criterion (RP: $\mu < 1$) [15]. The controller parameters are

$[K_{c1} = 0.94, \tau_{I1} = 187.3]$ and $[K_{c2} = 0.99, \tau_{I2} = 197.3]$. The performance bandwidth (ω_B^*) of 0.0025 *Hz* and a maximum allowable sensitivity peak (M) of 4 are both achieved. The implementation results of this PI controller in reference tracking and disturbance rejection are discussed in Section 6.

5.2 Robust Internal Model Controller design

Internal Model Control (IMC) is a very effective method of utilizing a process model for feedback control and requires minimal on-line computation. For a full discussion of IMC, see the monograph by Morari and Zafiriou [17]. Typically, IMC involves "inversion" of a portion of the model for use as a controller for the process. However, some portions of a linear process model cannot be inverted. These non-invertible factors include time delays and Right-Half-Plane (RHP) zeros. In addition, a process model that is not semi-proper cannot be inverted directly. A linear filter could be added to make the process model invertible. The filter parameters then are utilized in tuning the aggressiveness of the IMC controller for robust closed-loop performance.

The following "inner-outer" factorization for the stable process $G(s)$ follows the procedure described in [17]. The linear process transfer function can be written in terms of the state space matrices $\{A, B, C, D\}$ as:

$$G(s) = C(sI - A)^{-1}B + D = N(s)M(s)^{-1}$$

where $N(s)$ and $M(s)$ are stable. Additionally, $N(j\omega)^H N(j\omega) = I$. Given a factorization of D as $D = Q_I R_I$, the non-invertible portion of the process, $N(s)$, is given by:

$$N(s) = (C - Q_I\Phi)(sI - (A - BR_I^{-1}\Phi))^{-1}BR_I^{-1} + Q_I$$

The invertible part of the process, $M(s)^{-1}$, is:

$$M(s)^{-1} = \Phi(sI - A)^{-1}B + R_I$$

The operator Φ is given as:

$$\Phi = Q_I^T C + (BR_I^{-1})^T X$$

where X is the solution of the algebraic Riccati equation:

$$0 = (A - BR_I^{-1}Q_I^T C)^T X + X(A - BR_I^{-1}Q_I^T C) - X(BR_I^{-1})(BR_I^{-1})^T X$$

The state space description of $N(s)$ is:

$$A_N = A - BR_I^{-1}F \quad B_N = BR_I^{-1}$$
$$C_N = C - Q_I\Phi \qquad D_N = Q_I$$

For $M^{-1}(s)$, the state space matrices are given as:

$$A_M = A \quad B_M = B$$
$$C_M = \Phi \quad D_M = R_I$$

In the current study, the orthogonal matrix Q_I is selected as identity. The true plant whose linearized state space model is given in Equation 3 is strictly proper. For the purpose of the "inter-outer" factorization, the process has to be semi-proper. So, D is set to ϵI, where the scalar $\epsilon = 0.1$ here. Smaller values of ϵ give a better approximation of the true plant, but result in a controller that is sensitive to noise whereas larger values of ϵ results in increased plant-model mismatch. The $\epsilon = 0.1$ chosen in this study provided a good closed-loop performance while maintaining low sensitivity to measurement noise.

A schematic of the closed-loop system employing the "inner-outer" factorization based IMC controller is shown in Figure 11. The controller for the IMC formulation is the inverse of $M(s)$, the invertible portion of the process model. For offset free steady state reference tracking in all channels, the product of the controller gain and the process model gain must be identity. The current process model factorization does not guarantee this. It can conveniently be achieved by scaling the controller by $N(0)^{-1}$. Now, the non-invertible process model is $N(s)N(0)^{-1}$ and the invertible process model is $N(0)M^{-1}(s)$. The IMC controller becomes $M(s)N(0)^{-1}$. SISO IMC systems incorporate a scalar filter for strictly-proper process models so that the resulting controller is semi-proper and is realizable. In this multivariable case, the process model is already assumed to be semi-proper. Each of the error signals sent to the MIMO 2x2 IMC controller can be filtered by a first-order linear filter of the form, $F_i(s) = \frac{1}{\lambda_i s+1}$. This filter allows for tuning the aggressiveness of the controller to achieve desired robust closed-loop performance. In this study, $\lambda_i = 50\,sec$ are chosen. The resulting controller is stable and all closed-loop transfer functions are found to be stable. The performance bandwidth (ω_B^*) of 0.005 Hz and a maximum allowable sensitivity peak (M) of 3 are both achieved. Figure 12 shows the NP, RS and RP measures for the designed IMC controller. This controller has a μ-value of 0.99 satisfying the robust performance criterion (RP: $\mu < 1$) [15].

The process RHP zero is located at 0.034. The input direction corresponding to the RHP (as described in [2]) is: $[-0.69; 0.73]$ and the output direction is $[-0.73; 0.69]$. In the nominal case, the process is identical to the process model and the filter time constants are set to 0. The complementary sensitivity function, $T(s)$, for the nominal IMC system reduces to $N(s)N(0)^{-1}$. Ideally, $T(s)$ is identity at all frequencies. The presence of a RHP zero creates a performance limitation for the system. In [17], it is shown that $T(s)$ for a nonminimum phase system with a single zero can be arbitrarily selected so that only a single row deviates from identity. This implies that the performance degradation caused by the RHP zero can

be driven into a single output channel. The nominal complementary sensitivity function for the 2x2 four tank system with ideal performance in the first measurement is:

$$T_1(s) = \begin{bmatrix} 1 & 0 \\ \frac{\beta_1 s}{s+\zeta} & \frac{-s+\zeta}{s+\zeta} \end{bmatrix}$$

and the complementary sensitivity function for the system with ideal performance in the second measurement is:

$$T_2(s) = \begin{bmatrix} \frac{-s+\zeta}{s+\zeta} & \frac{\beta_2 s}{s+\zeta} \\ 0 & 1 \end{bmatrix}$$

where β_1 and β_2 are functions of the terms in the output zero direction. Significant interaction can occur when the values of β_i are large. For the given system, β_1 is 2.1 and β_2 is 1.9. This implies that choosing either input for ideal tracking in the nominal case will have essentially the same amount of interaction. This is an expected result due to the symmetric nature of the system. For the developed controller formulation, a first-order realization of nominal $T(s)$ is given as:

$$T(s) = \begin{bmatrix} \frac{5.82s+1}{32s+1} & \frac{42.74s}{42.74s+1} \\ \frac{42.74s}{42.74s+1} & \frac{-5.82s+1}{42.74s+1} \end{bmatrix}$$

This also demonstrates that the system and controller formulation is symmetric. Both output channels should demonstrate identical performance limitations and interactions. The implementation results of this IMC controller in reference tracking and disturbance rejection cases are discussed in Section 6.

5.3 Nominal H_∞ controller design

A mixed sensitivity H_∞ based controller is designed for the nominal four tank system. This controller is obtained by minimizing the following quantity:

$$\left\| \begin{bmatrix} W_p SR \\ W_u KSR \end{bmatrix} \right\|_\infty \tag{9}$$

where S is the sensitivity function, K is the controller, $R(= I)$ is the reference scaling matrix, and W_u is a filter to penalize the control action in the neighborhood of the desired bandwidth. In the current problem, W_u is chosen to be equal to I as there is no specific requirement on inputs other than maintaining them within ± 1. The controller thus designed will be referred to as the "nominal H_∞ controller" for the rest of this discussion.

A 6^th order controller is designed through the γ-iteration procedure using *hinfsyn* function in μ-toolbox in MATLAB^{TM} [18]. A performance bandwidth (ω_B^*) of 0.006 Hz and a maximum allowable sensitivity peak (M) of 2 were achieved through this controller design procedure. All closed-loop transfer functions with this controller were found to be stable, thus giving a nominal stable closed-loop controller. To satisfy certain rank conditions in H_∞ controller synthesis, G_d must be semi-proper [18]. If the disturbance is assumed to affect the measured levels directly, *i.e.*, $G_d = I$, then the controller syntheses for the disturbance rejection and reference tracking are equivalent with $R = I$ in Equation 9. This is a reasonable assumption as the amplitude ratio of G_d is always less than 1 with a steady state value of 0.9. However, the achieved bandwidth will be conservative for the disturbance rejection case.

The sensitivity and input constraint plots are shown in Figure 13. It can be seen that the input constraints are not violated for this controller ($\|W_u KSR\|_\infty < 1$). The robust performance of this controller is characterized using μ-analysis. This involves a formulation of the performance problem as an appropriate robust stability problem with suitably defined uncertainty structure [2, 19]. The resulting uncertainty structure is block diagonal and can be represented in the M-Δ structure utilized for μ-analysis [2, 20]. Figure 14 shows that this controller satisfies the nominal performance (NP: $\|W_p S\|_\infty < 1$) and robust stability (RS: $\|W_I T\|_\infty < 1$) criteria. To guarantee robust performance the structured singular value (μ)

has to be less than 1 [15]. The nominal H_∞ controller does not satisfy this robust performance criterion. The μ-value corresponding to the plot in Figure 14 is 1.25. This indicates that all the uncertainty blocks considered in the RP problem should be decreased in magnitude by a factor of 1.25 in order to guarantee robust performance, *i.e.*, both plant uncertainty and performance specification should be reduced by a scaling factor of 1.25. The *skewed-*μ value is computed to determine the level of plant uncertainty for which the controller is robust without the loss of achieved nominal performance. This analysis allows scaling of a particular source of uncertainty (plant uncertainty, in this case) so that the robust performance criterion is satisfied [2]. The *skewed-*μ value of the system with the nominal H_∞ controller is found to be 2.1. This means that the designed H_∞ controller would provide robust performance to approximately 48% of the level of plant input uncertainty considered in this study. The design of a controller that is robust to the specified level of plant uncertainty is presented in the next section.

5.4 Robust H_∞ controller design

A design of the μ-analysis based H_∞ controller that achieves robust performance is presented in this section [1, 15]. Using the standard D-K iteration procedure [19, 15], a $28th$ order controller is obtained after 3 iterations. This controller has a μ-value of 0.99. The computational tools available in the μ-toolbox in MATLAB^{TM} are utilized in the controller design [19]. The performance bandwidth (ω_B^*) of 0.007 Hz and a maximum allowable sensitivity peak (M) of 2 are both achieved. The resulting controller is stable and all closed-loop transfer functions are found to be stable. The nominal performance, robust stability, and robust performance indices for this controller are shown in Figure 15.

5.5 Input constraints

In all the the controller designs presented, input constraints are not explicitly accounted for, *i.e.*, the controller design did not incorporate the term $W_u KSR$ in the nominal performance measure. For all the three designed controllers, $\bar{\sigma}(KS)$ increases to values greater than 1 within the bandwidth frequency. This derivative action in the bandwidth frequency could result in an input of size greater than 1 for appropriate changes in the reference. On the other hand, the performance bandwidth degraded considerably when the input size constraints were introduced into the μ-analysis based H_∞ controller design. Similar results apply to the PI and IMC controllers designed here. As an alternative, a first-order pre-filter could be implemented on the setpoint changes to overcome this issue. The time constant of the setpoint pre-filter is based on the corner frequency of $\overline{\sigma}(KSR)$, and is set to 50 *sec* for the current problem. Such filter is not necessary for the disturbance rejection problem as G_d is found to be a sufficient pre-filter for the disturbance. However, in practice, the controllers provided better performance with the inputs constrained to remain within $25 - 75\%$ than when the reference filter is employed. This is expected as the reference filter significantly detunes the closed-loop response whereas "clipping" the inputs does not degrade closed-loop performance considerably as long as the input is not saturated within the achieved bandwidth.

6 Results and Discussion

To validate the performance of the designed controllers, closed-loop simulations were conducted prior to implementation on the experimental system. The simulation and implementation results are discussed in the next two subsections.

6.1 Simulation results

For the purpose of simulation, the "real" process is simulated by the nonlinear state space model described in equation 1. A perturbed system is simulated by increasing the parameters $\gamma_1, \gamma_2, k_1,$ and k_2 by 10%. The setpoints were perturbed in the direction of the minimum singular value of the plant (increase in h_1 and equal decrease in h_2). Seperate simulations were performed for each of the robust PI, robust IMC and μ-analysis based H_∞ controllers. Reference tracking results for the perturbed system with the robust controller are shown in Figure 16. The robust IMC and H_∞ controllers provided better reference tracking performance than the decentralized PI controller. The pump levels, as computed by the controllers, are not maintained within the actuator constraints. However, clipping the pump inputs provided good performance without saturating the pumps at steady state. For the PI and the H_∞ controllers, the input constraints are active for a brief period when the setpoint changes. However, the process contains sufficient input capacity to reach the setpoint without saturating the pumps. Although the designed H_∞ and IMC controllers did not contain integral action (as defined theoretically), the performance weight W_p is designed such that only a very small offset (0.1%) is tolerated at steady state. This is sufficiently close to integral action and could result in reset windup if the reference changes were introduced in such a dynamic manner as to continuously "excite" only the high frequency components of the controller resulting in input constraint violation. Such reference trajectories were not explored in this study.

For the disturbance rejection case, a 10 minute long leak in Tank 4 is simulated. All the three controllers provided desired performance with similar closed-loop peak change in tank levels. The results for the disturbance rejection case are shown in Figure 17. All the contollers attenuated the peak change in the measured levels by 60% when compared to open-loop case. In the simulations, IMC and the H_∞ controllers have similar disturbance rejection performance. The pump levels were more oscillatory when the PI controller is

employed. Pump inputs were maintained within the constraints. An additional pre-filter was not required in this case as the filtering performed by G_d was found to be sufficient.

6.2 Experimental results

Controller implementation was successfully carried out using the four tank experimental apparatus. In order to incorporate a controller more advanced than P, PI, or PID, the Dynamic Data Exchange interface was used to link MATLAB with Freelance^{TM}, the software interface to the laboratory experiment and the control hardware. The state space controller was discretized using one second intervals. The levels in the bottom tanks were sampled every second and the computed control move was implemented. The closed-loop time constant of the system is approximately 2 orders of magnitude larger than the sample time, hence, no discretization effects were observed.

Separate experiments were conducted for setpoint tracking and disturbance rejection. The setpoint changes were made in the direction of the minimum singular value of the plant, to verify that the inputs are maintained within the constraints. Figure 18 shows the setpoint tracking results for the PI, IMC and H_∞ controllers. As indicated by the simulations with the perturbed plant, the decentralized PI controller provided more oscillatory changes in the tank levels and the pump inputs when implemented on the experimental system. However, the IMC and the H_∞ controller performed similarly with the former being more sensitive to noise. As seen in Figure 18, the step change in the reference produces a derivative action on the inputs to the pumps. However, these input moves were constrained to $\pm 25\%$ prior to communicating with the experimental hardware. This provides better performance than reference pre-filtering in this problem, as the designed pre-filter adds considerable additional lag to system degrading the closed-loop performance. The settling time of the tank levels is approximately $250 - 275$ *seconds*.

For the disturbance rejection problem, a leak is introduced into the Tank 4 by turning the submersible pump on. The leak is shut after 10 minutes by turning the submersible pump off. The closed-loop performance of the controllers for the disturbance rejection case is shown in Figure 19. All the three controllers do provide reasonable performance in rejecting the flow disturbances. The open-loop change in the measured levels is 3.5 cm and the peak level change in the closed-loop is 2 cm for IMC and 1.75 cm for the H_∞ and PI controllers.

The PI, IMC and H_∞ controllers provide robust performance with different bandwidths and have different robust performance characteristics as is evident from the corresponding RP measures in Figures 10, 12 and 15. The IMC and H_∞ controllers provided similar performance for both reference tracking and disturbance cases. This similarity is in tune with the similarity of corresponding measures for IMC and H_∞ controllers (Figures 12 and 15f). For disturbance rejection problem, all the three controllers provide similar performance. Inputs to the closed-loop system, *i.e.*, reference $\boldsymbol{r}$, and disturbance $\boldsymbol{d}$, need to sufficiently "excite" the system so that various controllers can be differentiated from the closed-loop performance. It is plausible that the disturbance dynamic (G_d) is effectively "pre-filtering" the leak via submersible pump. This could result in similar performance of all the controllers in the disturbance rejection case by not "exciting" the system "fast enough". However, the rapid setpoint changes excites the system sufficiently to produce different closed-loop dynamic responses for different controllers.

7 Conclusions

The design and implementation of robustly performing PI, IMC and H_∞ controllers for an experimental four tank process is presented. Flow disturbances are introduced in the upper level tanks to modify the original process. Nonlinear optimization is used to identify the model parameters from the dynamic experimental data. The inverse response in the system

is adequately captured using the nonlinear model parameter identification. The achievable performance is characterized using acceptable control analysis. Lumped unstructured input uncertainty is found to be sufficient to model various effects of the parametric and actuator uncertainties in the system. A relay tuning based decentralized PI controller, a inner-outer factorization based IMC algorithm, and a μ-analysis based H_∞ optimal controller are designed. Implementation results on the physical system show that all the three controllers provide stable and desired performance for both reference tracking and disturbance rejection. The IMC and H_∞ controllers performed similarly and provide better performance than the decentralized PI controller for the reference tracking problem. To improve the closed-loop performance on the experimental system, the pump settings were constrained to remain within $25\% - 75\%$ rather than employing a reference pre-filter. The controller design methods employed in this work are expected to perform well for any of the linear time-invariant system included in the uncertainty characterization. However, the experimental system is inherently nonlinear and not all nonlinear dynamics involving piping overheads and stochastic nature of the apparatus is captured by the nonlinear state space model employed in this study(equation 1). Performance degradation from simulation to implementation may be due to the inherent stochastic behavior of the apparatus which varies the steady states from one operation to another, potentially placing the system outside the uncertainty characterization area for which the controller is designed.

Acknowledgements

The authors gratefully acknowledge support from the Office of Naval Research, USA (Grant NOOO-14-96-1-0695) and University of Delaware Process Control and Monitoring Consortium. The authors also acknowledge the helpful comments by the reviewers of this manuscript in shaping the focus of the paper.

References

[1] Doyle, J. C. Analysis of Feedback Systems with Structured Uncertainties. *IEEE Proc., Part D*, **1982**, 129(6), 242–250.

[2] Skogestad, S.; Postlethwaite, I. *Multivariable Feedback Control*; John Wiley & Sons: New York, 1996.

[3] Smith, R. S.; Doyle, J. C. The Two Tank Experiment: A Benchmark Control Problem. in *Proc. American Control Conf.*, Atlanta, GA, 1988, 2026–2031.

[4] Braatz, R.; Tyler, M.; Morari, M.; Pranckh, F.; Sartor, L. Identification and Cross-directional Control of Coating Processes. *AIChE J.*, **1992**, 38, 1329–1339.

[5] Budman, H.; Webb, C.; Holcomb, T.; Morari, M. Robust Inferential Control for a Packed-Bed Reactor. *Ind. Eng. Chem. Res.*, **1992**, 31, 1665–1679.

[6] Amann, N.; Allgöwer, F. μ-suboptimal Design of a Robustly Performing Controller for a Chemical Reactor. *Int. J. Control*, **1994**, 59(3), 665–687.

[7] Heiming, B. Presentation of a Laboratory 3-Tank System. COSY-workshop, Valencia. Oct. 1996, URL: http://www.tu-hardburg.de/rts/software/cosy/.

[8] Johansson, K. H. Relay Feedback and Multivariable Control. PhD Dissertation, Lund Institute of Technology, Lund, Sweden, 1997.

[9] Gatzke, E. P.; Vadigepalli, R.; Meadows, E. S.; Doyle III, F. J. Experiences with an Experimental Project in a Graduate Control Course. *Chem. Eng. Educ.*, **1999**, 33(4), 270–275.

[10] Dai, L.; Åström, K. J. Dynamic Matrix Control of a Quadruple Tank Process. In *Proceedings of the 14th IFAC*, Beijing, China, 1999, 295–300.

[11] Johansson, K. J.; Nunes, J. L. R. A Multivariable Laboratory Process with an Adjustable Zero. In *Proc. American Control Conf.*, Philadelphia, PA, 1998, 2045–2049.

[12] Gatzke, E. P.; Meadows, E. S.; Wang, C.; Doyle III, F. J. Model Based Control of a Four–tank System. *Comput. Chem. Eng.*, **2000**, 24, 1503–1509.

[13] Holt, B. R.; Morari, M. Design of Resilient Processing Plants VI – The Effect of Right Plant Zeros on Dynamic Resilience. *Chem. Eng. Sci.*, **1985**, 40, 5–749.

[14] Ljung, L. *System Identification: Theory for the User*; P T R Prentice Hall: Englewood Cliffs, NJ, 1987.

[15] Doyle, J. C.; Chu, C. C. Matrix Interpolation and H_∞ Performance Bounds. In *Proc. American Control Conf.*, Boston, MA, 1985, 129–134.

[16] Åström, K.; Hagglund, T. Automated Tuning of Simple Regulators with Specifications on Phase and Amplitude Margins. *Automatica*, **1984**, 20, 645.

[17] Morari, M.; Zafiriou, E. *Robust Process Control*; Prentice-Hall: Englewood Cliffs, NJ, 1989.

[18] Doyle, J. C.; Glover, K.; Khargonekar, P. P.; Francis, B. A. State–Space Solutions to Standard H_2 and H_∞ Control Problems. *IEEE Trans. Aut. Control*, **1989**, 34(8), 831–847.

[19] Balas, G. J.; Doyle, J. C.;Glover, K.;Packard, A.; Smith, R. *μ-Analysis and Synthesis Toolbox User's Guide*; The Mathworks: Natick, MA, 1995.

[20] Packard, A.; Doyle, J. C. The Complex Structured Singular Value," *Automatica*, **1993**, 29(1), 71–109.

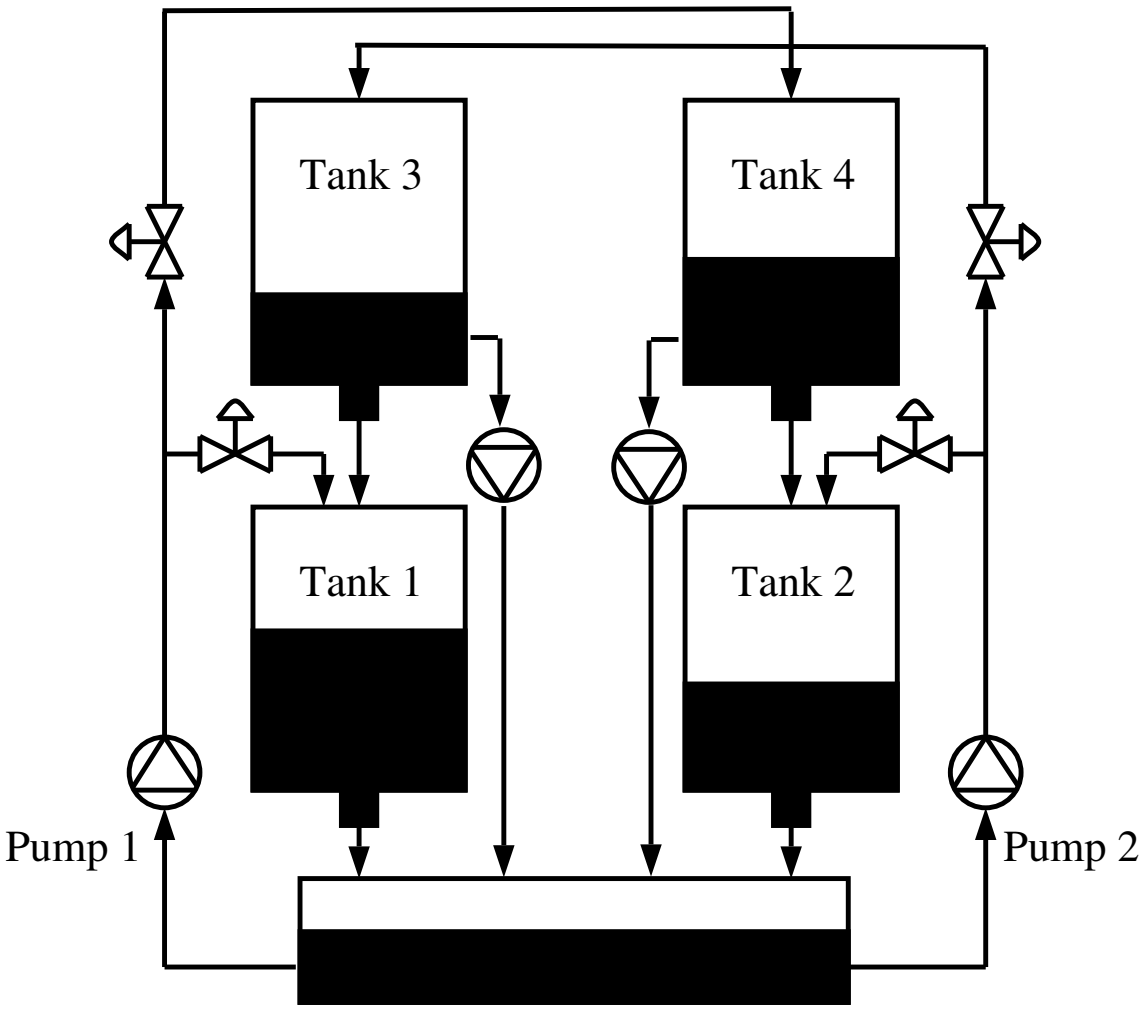

Figure 1: Schematic of the four interconnected tank system. The liquid levels in Tank 1 and Tank 2 are measured.

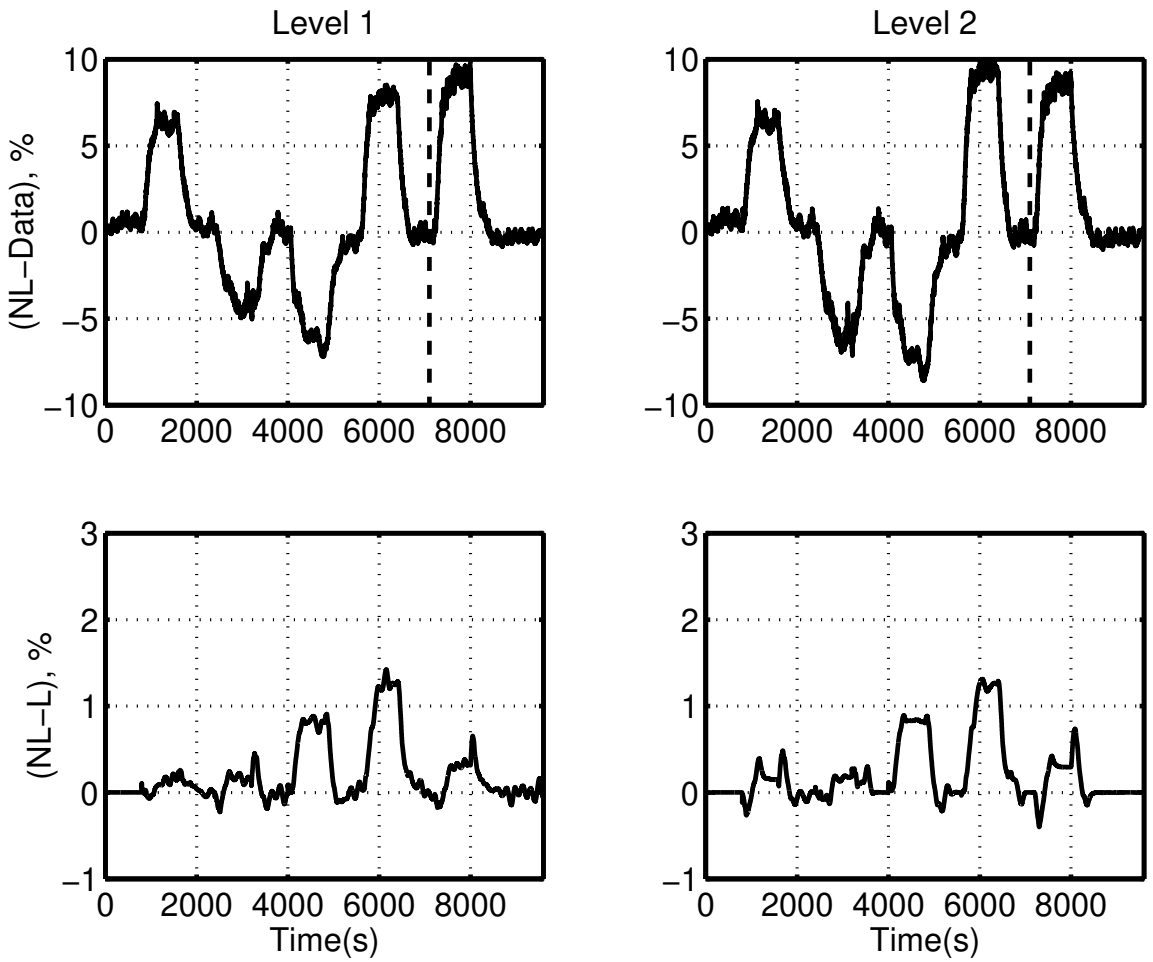

Figure 2: Residuals between experimental data, nonlinear model and linear approximations: (top) nonlinear model versus experimental data. The vertical line separates the data used for parameter estimation and model validation; (bottom) nonlinear versus linearized model.

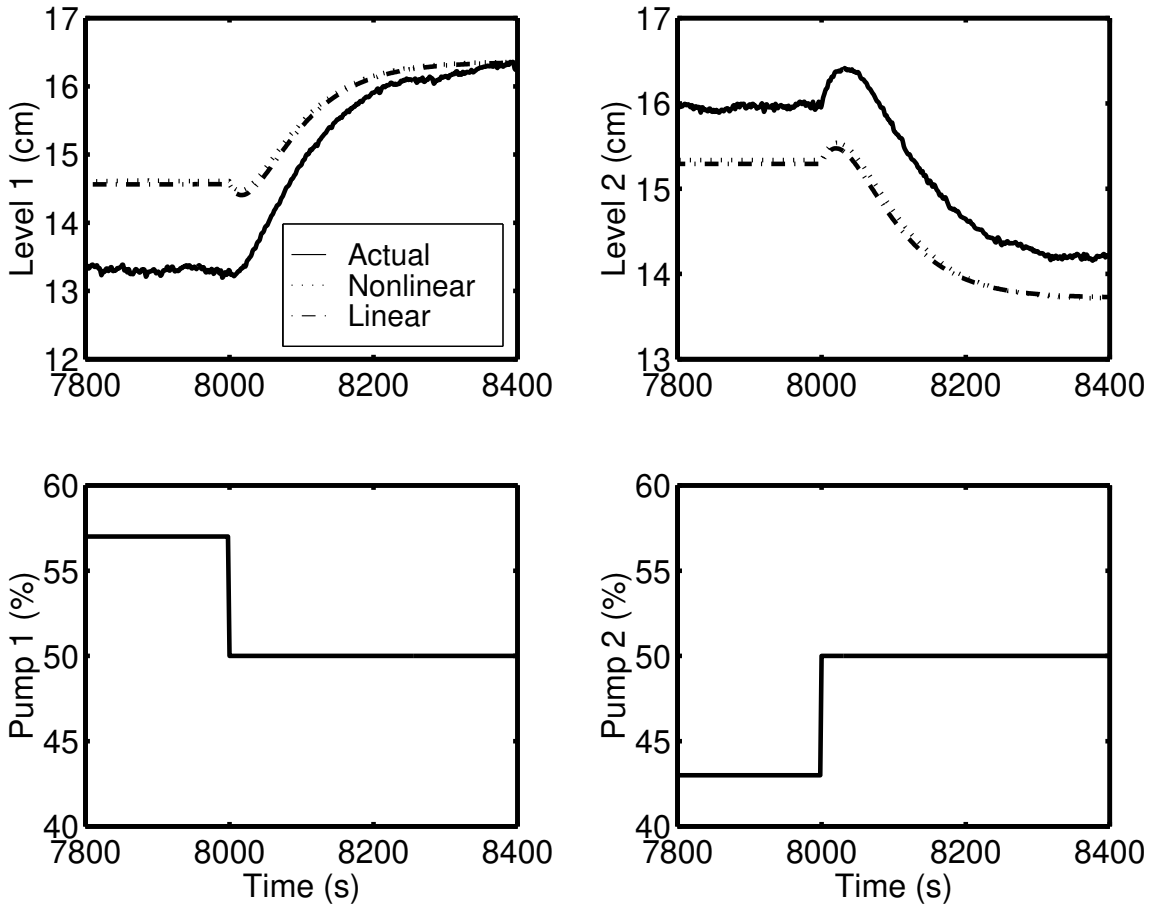

Figure 3: Validation of linearization and nonlinear models with experimental step data.

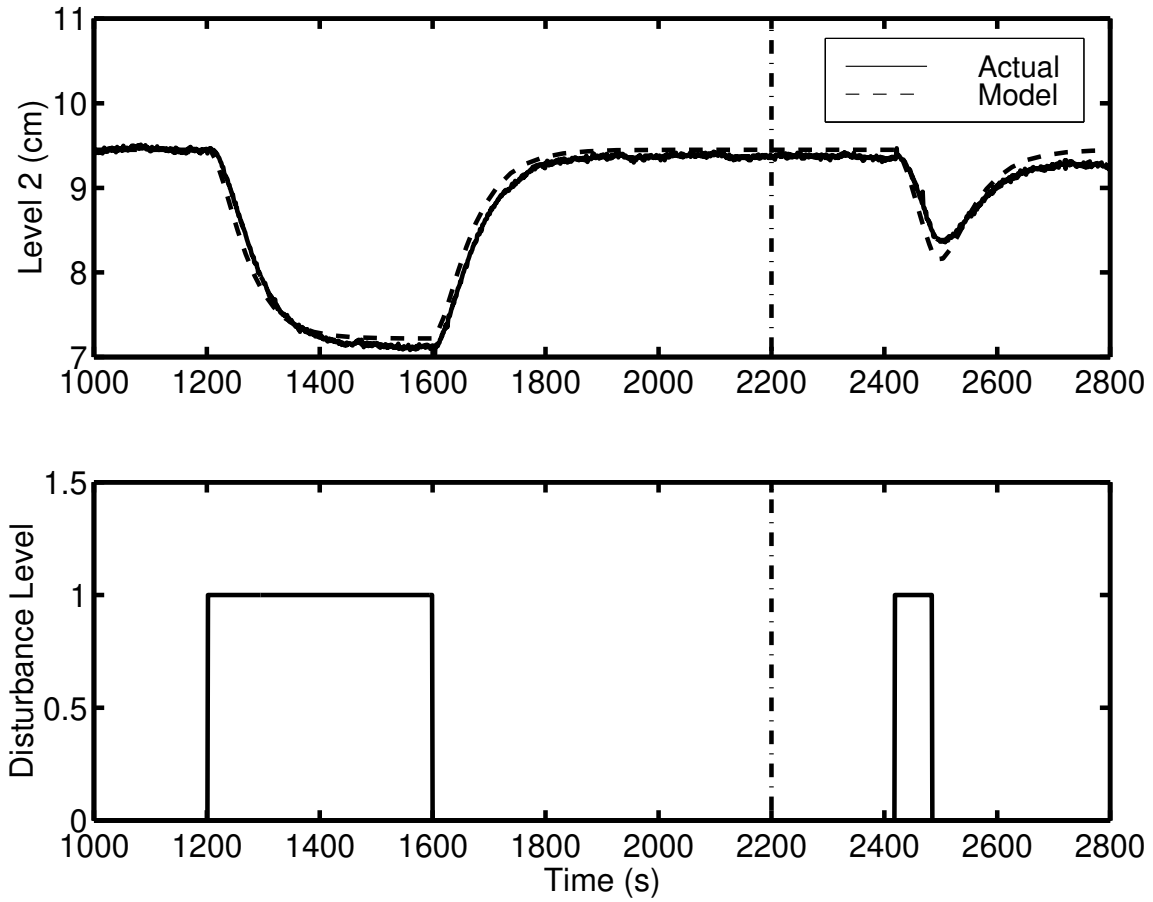

Figure 4: Identification of linear disturbance model with experimental pulse data. The vertical line separates the identification and validation data records.

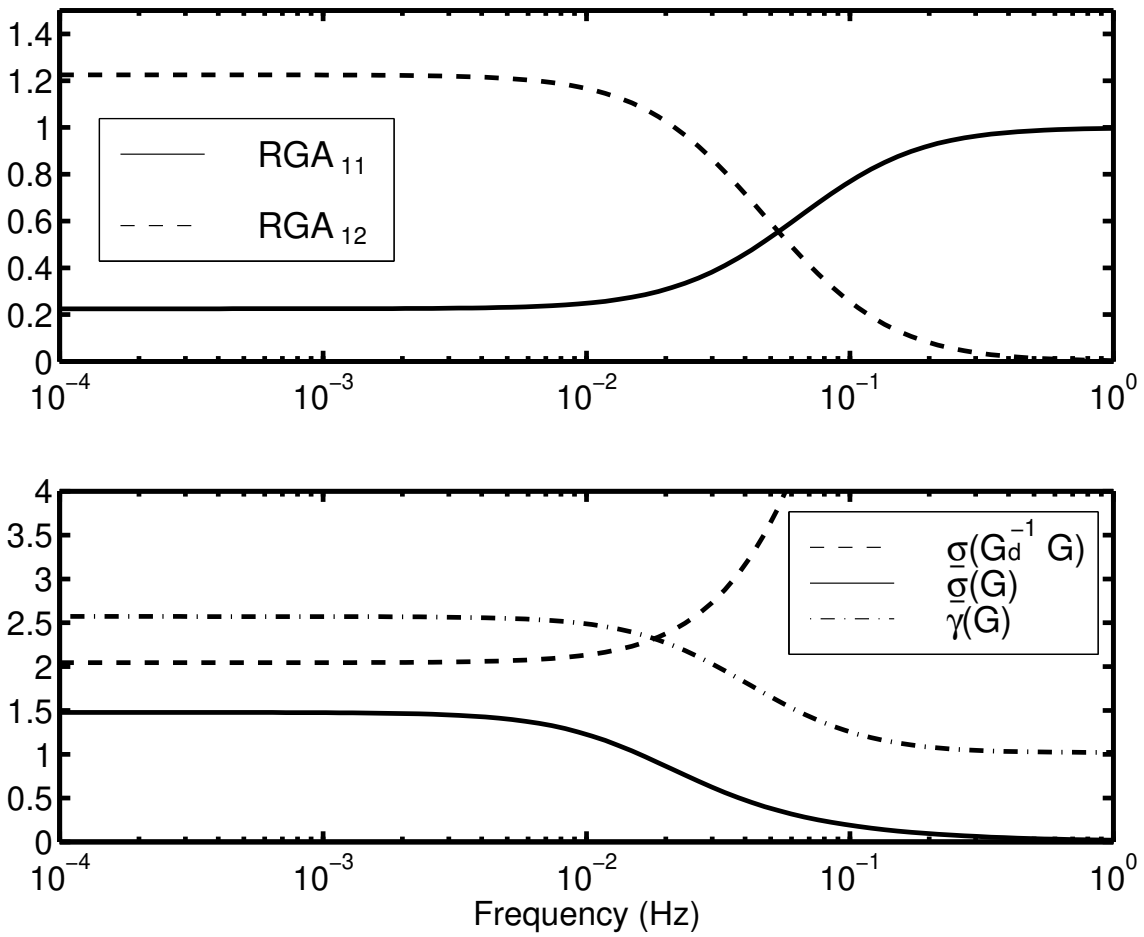

Figure 5: Input-output controllability analysis: RGA(G), $\underline{\sigma}(G)$ and $\underline{\sigma}(G_d^{-1}G)$. Bandwidth for reference tracking is 0.015 *Hz*. Perfect control for disturbance rejection requires $\underline{\sigma}(G_d^{-1}G) \geq 1$, $\forall\omega$.

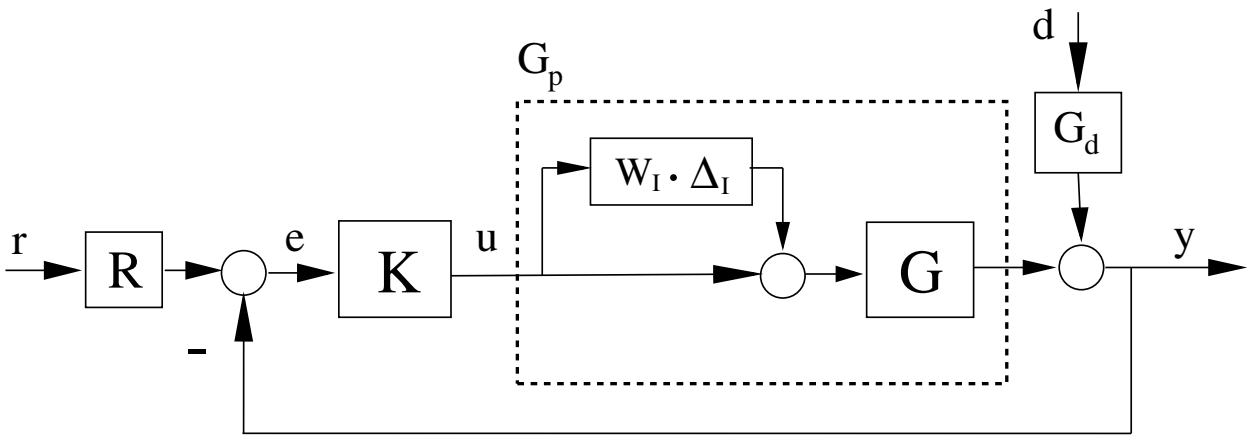

Figure 6: Block diagram of the closed-loop system with the real process G_p represented using a lumped unstructured multiplicative input uncertainty structure.

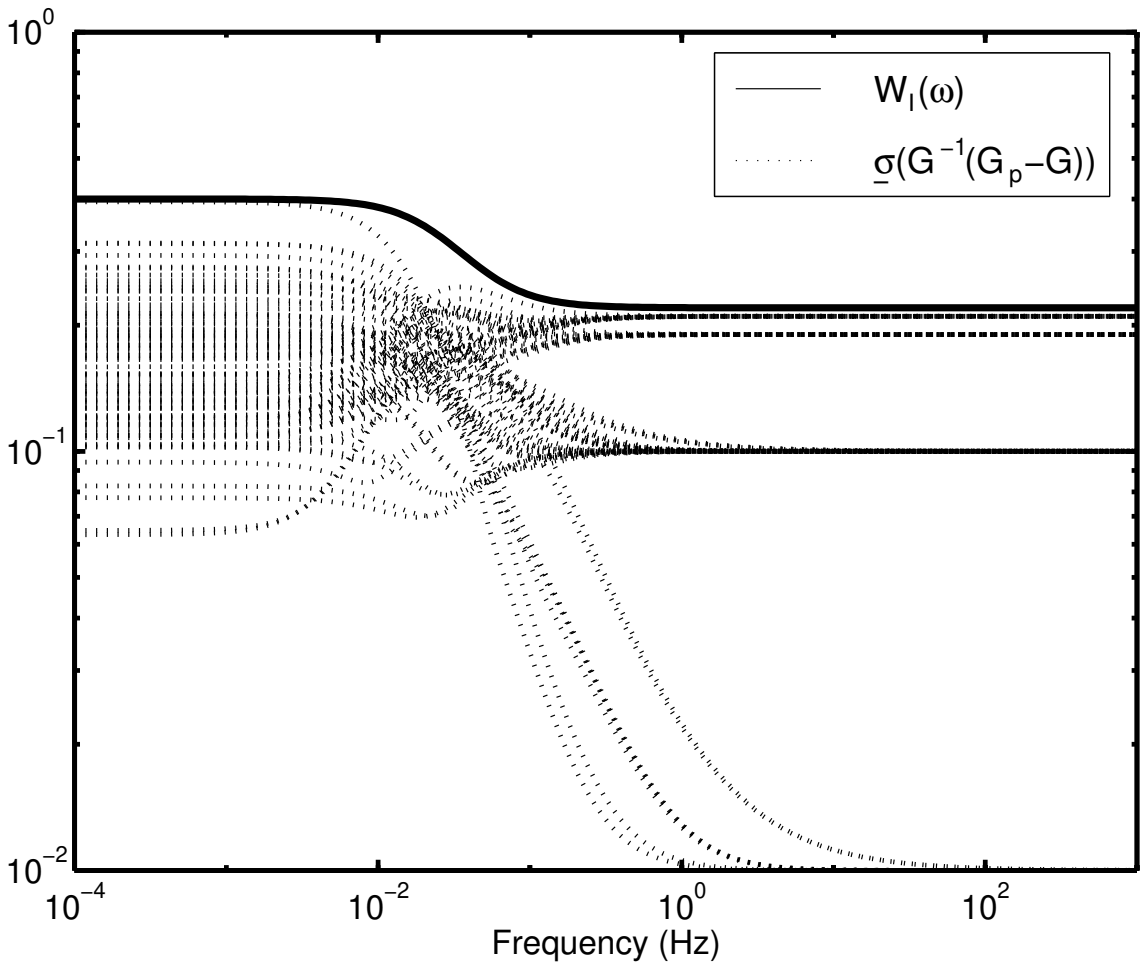

Figure 7: Input multiplicative uncertainty weight, W_I, as an upper bound on the process uncertainty due to $\pm 10\%$ variation in parameters γ_1, γ_2, k_1 and k_2.

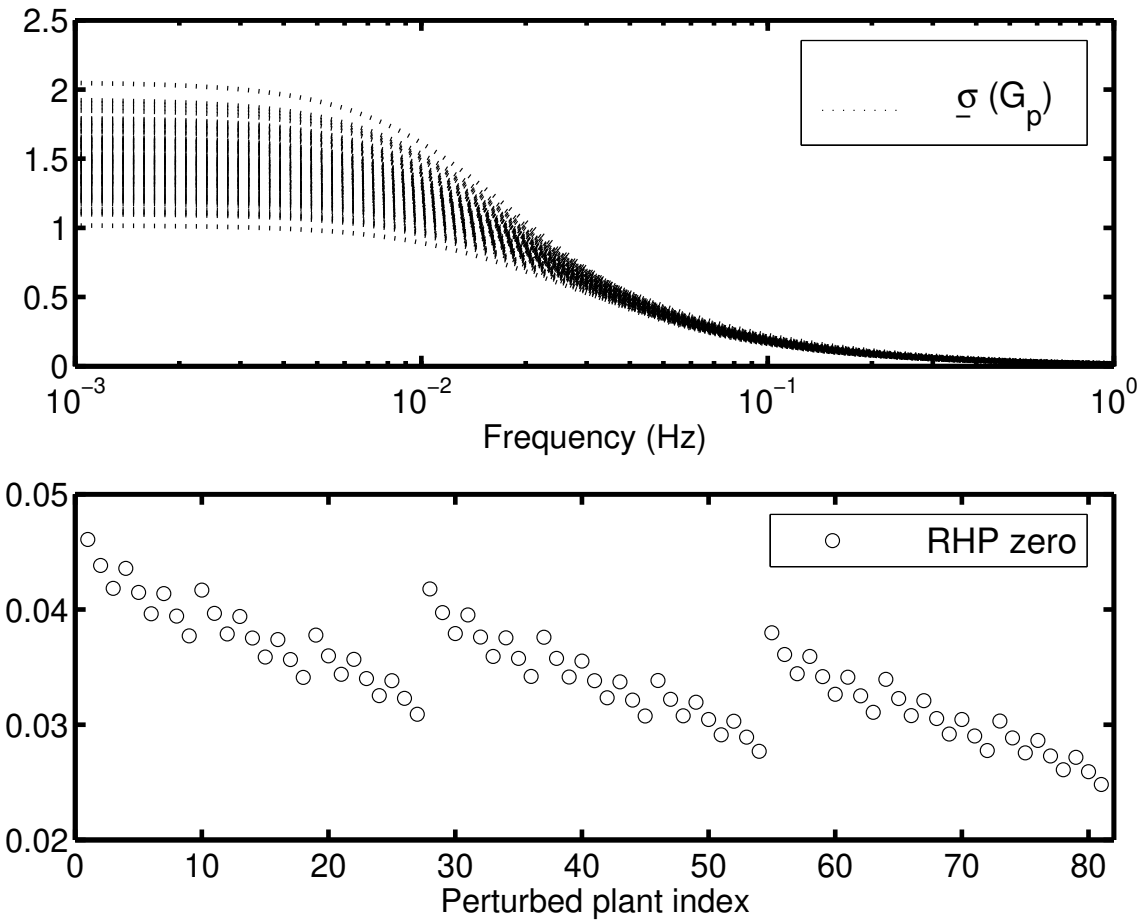

Figure 8: Variation in $\underline{\sigma}(G)$ and the RHP zero location due to $\pm 10\%$ variation in parameters γ_1, γ_2, k_1 and k_2.

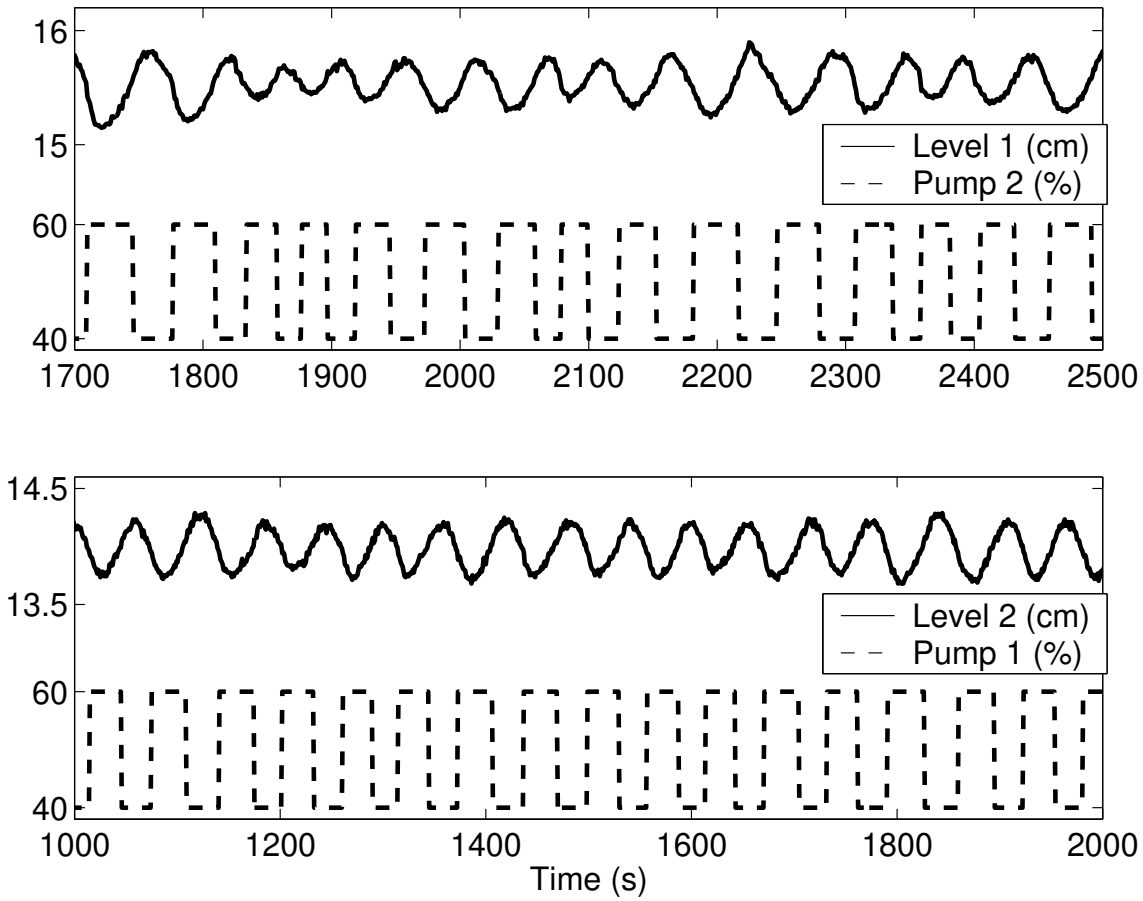

Figure 9: Input-output data utilized for relay tuning of two SISO PI controllers. The pairing is $(y_1 - u_2)$ and $(y_2 - u_1)$.

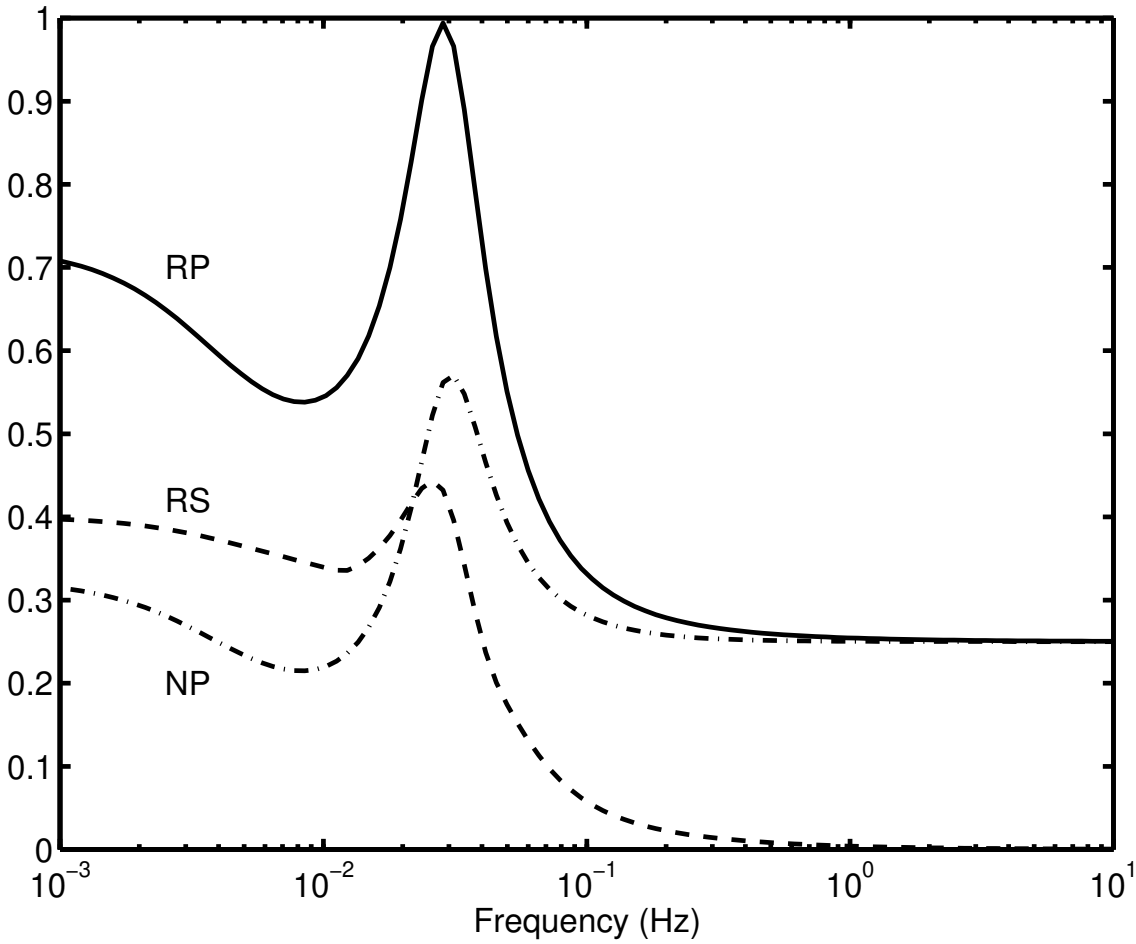

Figure 10: Nominal Performance (NP), Robust Stability (RS) and Robust Performance (RP) measures for the decentralized PI controller. The structured singular value, μ, is 0.99 as exhibited by the magnitude of the RP measure. A controller bandwidth of 0.0025 *Hz* and peak sensitivity value of 4 is achieved.

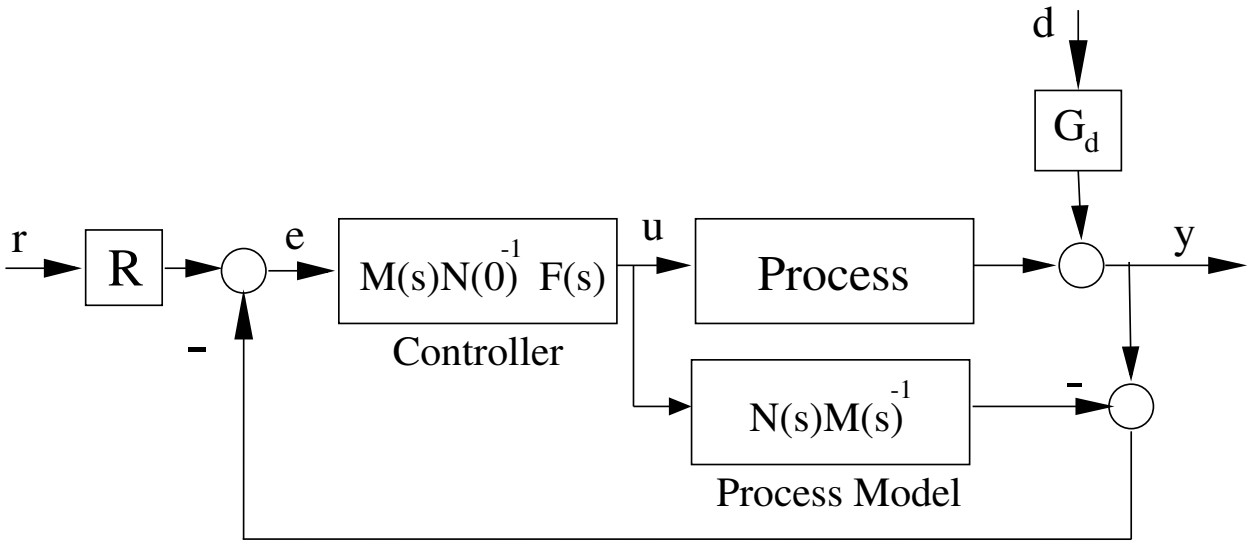

Figure 11: Block diagram of the closed-loop system with the Internal Model Control (IMC) structure. Note the "inner-outer" factorization of the plant $G(s)$ into the invertible portion $M(s)^{-1}$ and the non-invertible portion $N(s)$. $F(s)$ is the filter utilized in tuning the aggresiveness of the controller to achieve desired robust closed-loop performance.

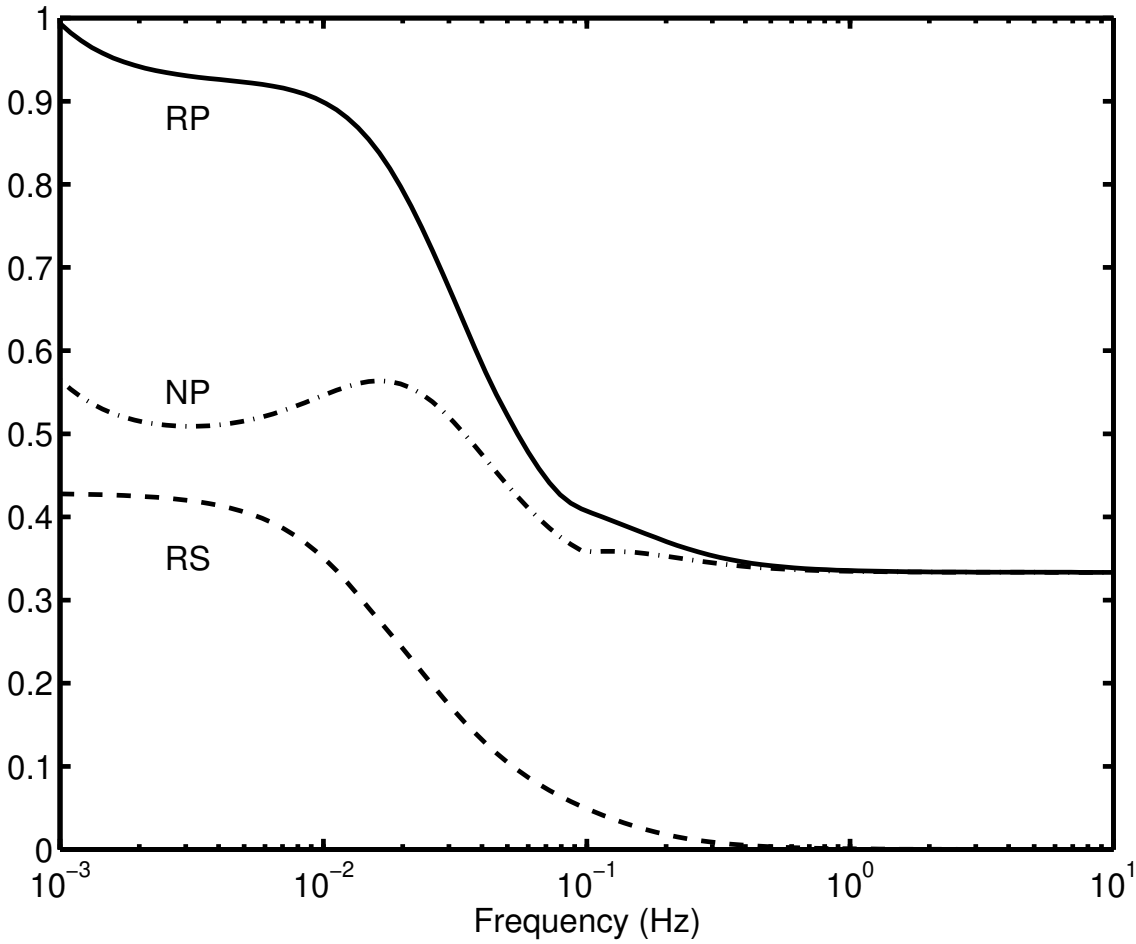

Figure 12: Nominal Performance (NP), Robust Stability (RS) and Robust Performance (RP) measures for the Internal Model Controller. The structured singular value, μ, is 0.99 as exhibited by the magnitude of the RP measure. A controller bandwidth of 0.005 *Hz* and peak sensitivity value of 3 is achieved.

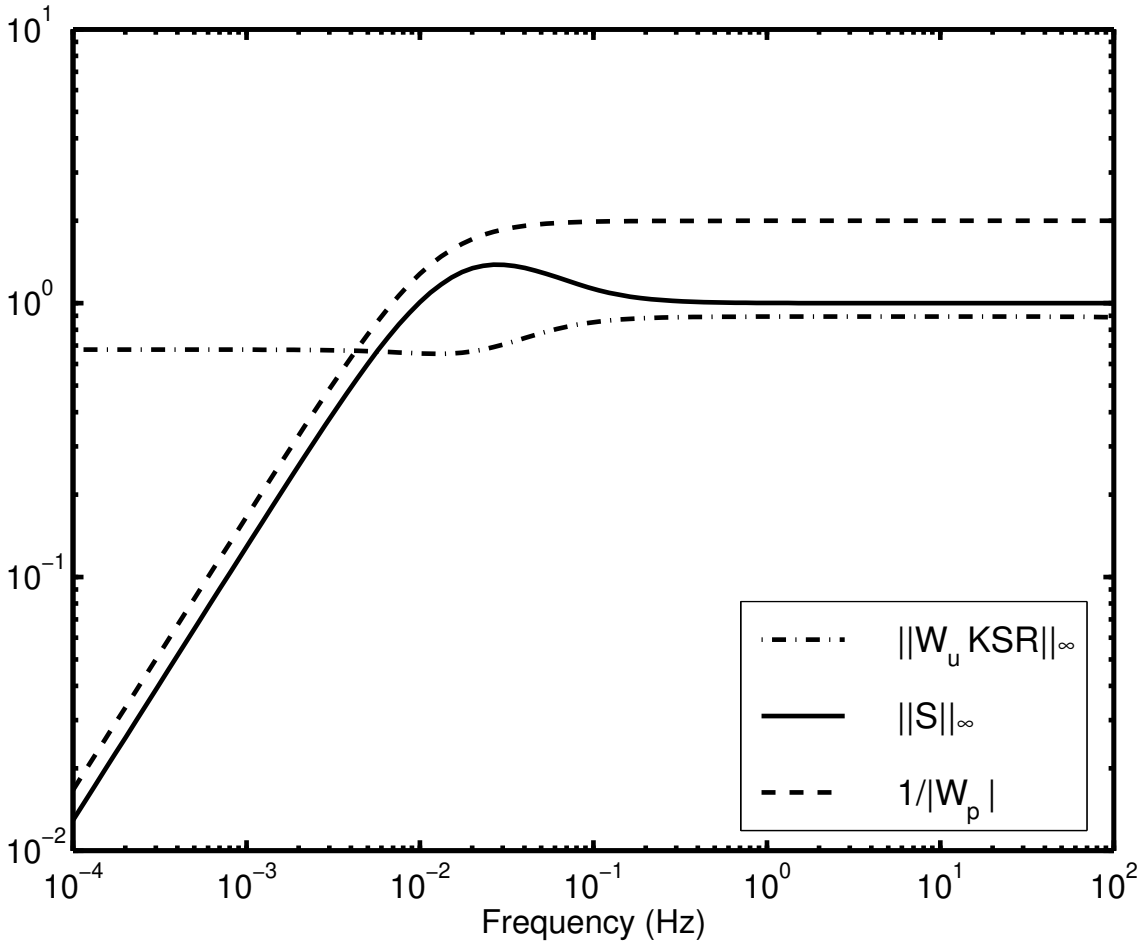

Figure 13: Sensitivity function and input constraints for the nominal system with the nominal H_∞ controller. Input constraints require that $\|W_u KSR\|_\infty < 1$. A controller bandwidth of 0.007 *Hz* and peak sensitivity value of 2 is achieved.

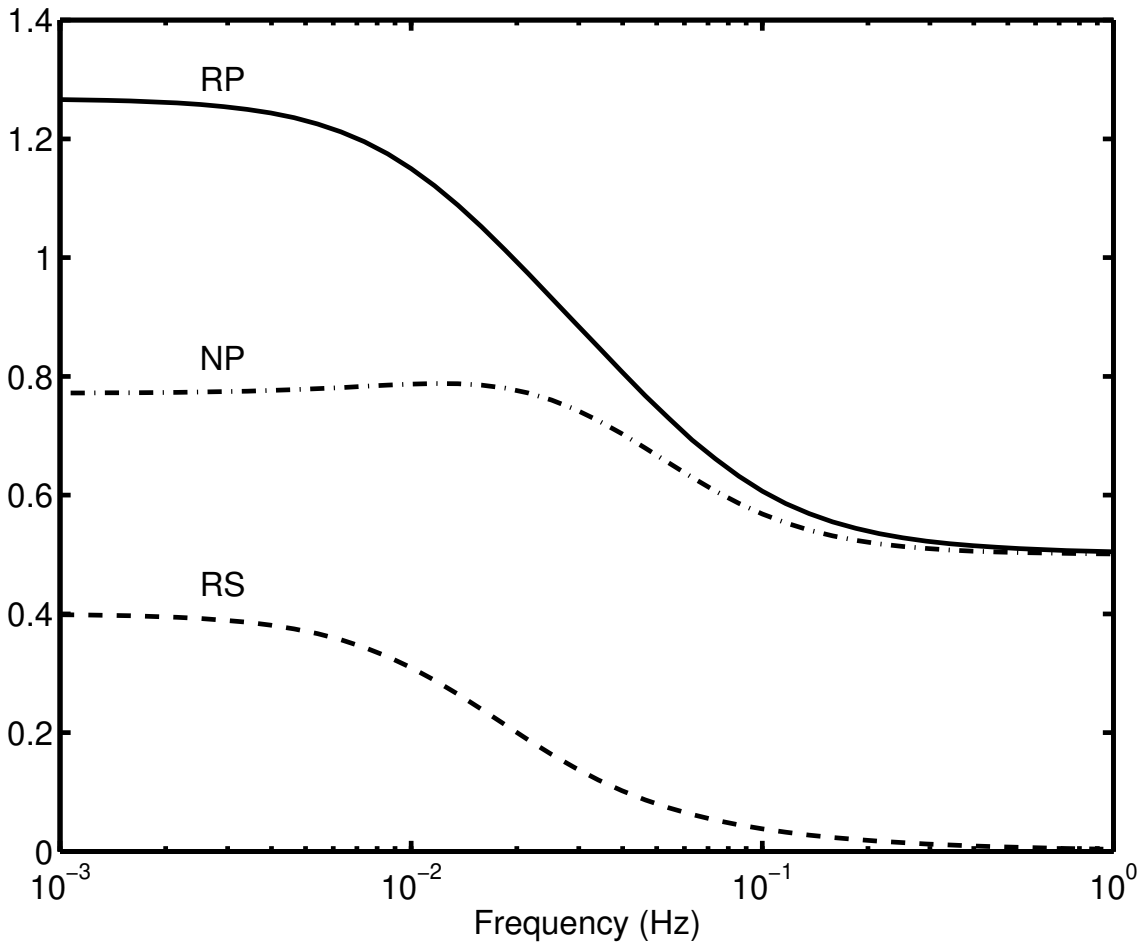

Figure 14: Nominal Performance (NP), Robust Stability (RS) and Robust Performance (RP) measures for the nominal H_∞ controller. The structured singular value, μ, is 1.25 as exhibited by the magnitude of the RP measure. A controller bandwidth of 0.006 *Hz* and peak sensitivity value of 2 is achieved.

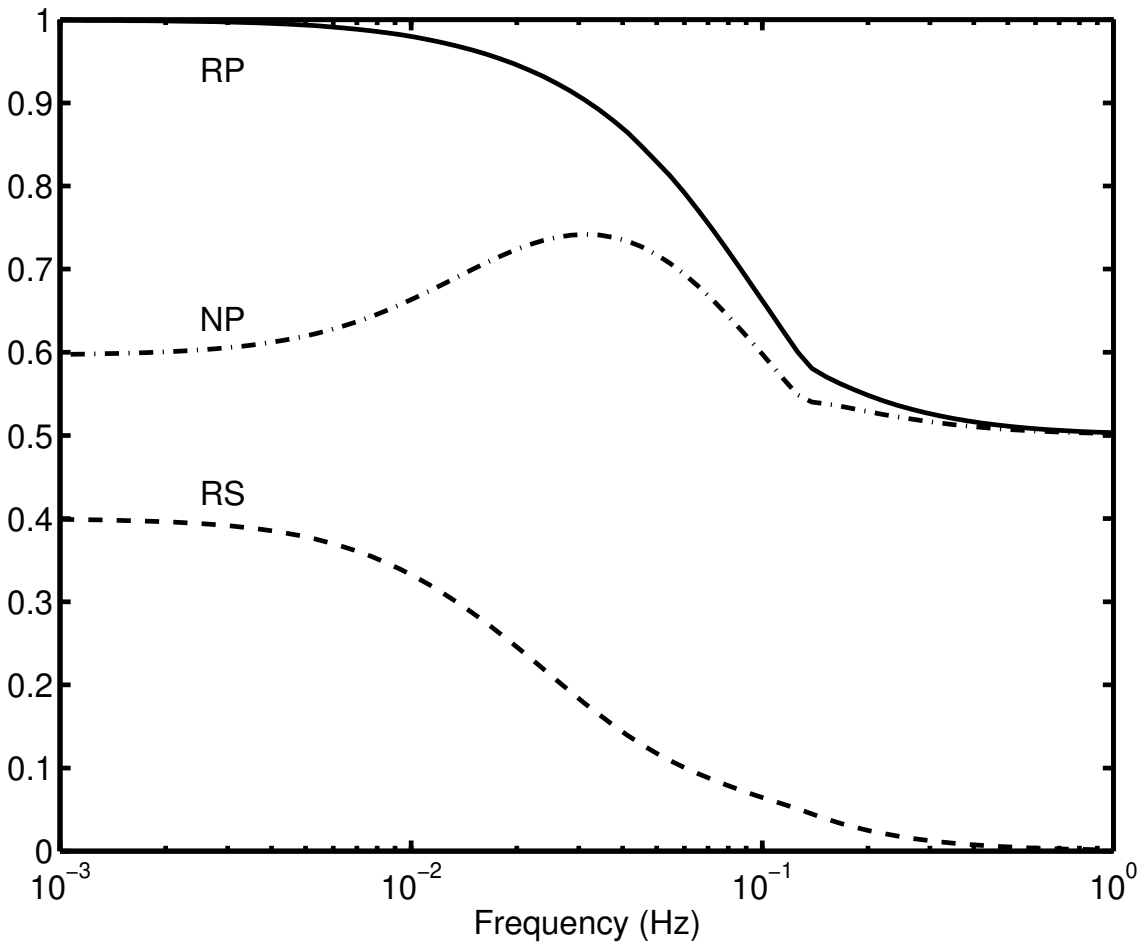

Figure 15: Nominal Performance (NP), Robust Stability (RS) and Robust Performance (RP) measures for the μ-analysis based H_∞ controller. The structured singular value, μ, is 0.99 as exhibited by the magnitude of the RP measure.

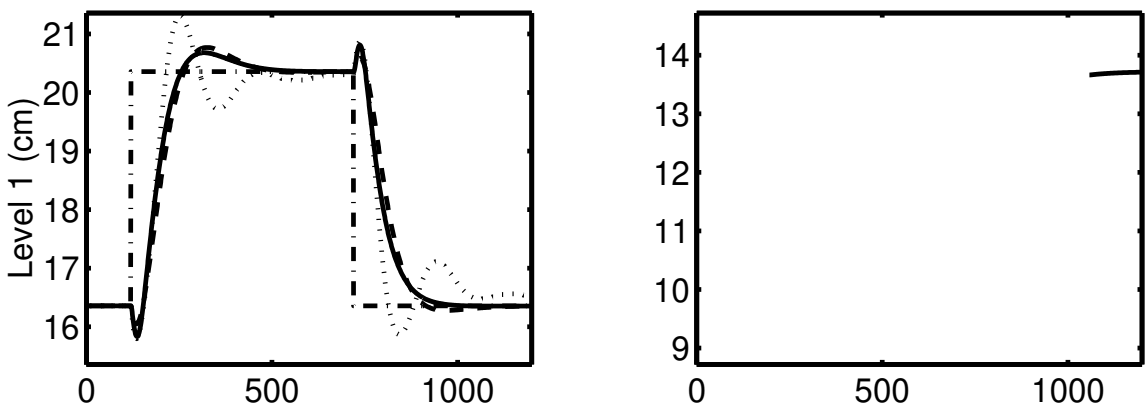
Level 1 (cm)
21
20
19
18
17
16
0
500
1000
14
13
12
11
10
9
0
500
1000